Computers and Mathematics with Applications 168 (2024) 162–173

Contents lists available at ScienceDirect

Computers and Mathematics with Applications

journal homepage: www.elsevier.com/locate/camwa

Companion-based multi-level finite element method for computing multiple solutions of nonlinear differential equations

Wenrui Hao [a], Sun Lee [a], Young Ju Lee [b,*]

[a] Department of Mathematics, Penn State, 16802 PA, State College, USA
[b] Department of Mathematics, Texas State, 78666 TX, San Marcos, USA

ARTICLE INFO

Keywords:
Elliptic semilinear PDEs
Nonlinear ODEs
Finite element method
Multiple solutions
Boundary conditions

ABSTRACT

The utilization of nonlinear differential equations has resulted in remarkable progress across various scientific domains, including physics, biology, ecology, and quantum mechanics. Nonetheless, obtaining multiple solutions for nonlinear differential equations can pose considerable challenges, particularly when it is difficult to find suitable initial guesses. To address this issue, we propose a pioneering approach known as the Companion-Based Multilevel Finite Element Method (CBMFEM). This novel technique efficiently and accurately generates multiple initial guesses for solving nonlinear elliptic semi-linear equations containing polynomial nonlinear terms through the use of finite element methods with conforming elements. As a theoretical foundation of CBMFEM, we present an appropriate and new concept of the isolated solution to the nonlinear elliptic equations with multiple solutions. The newly introduced concept is used to establish the inf-sup condition for the linearized equation around the isolated solution. Furthermore, it is crucially used to derive a theoretical error analysis of finite element methods for nonlinear elliptic equations with multiple solutions. A number of numerical results obtained using CBMFEM are then presented and compared with a traditional method. These not only show the CBMFEM's superiority, but also support our theoretical analysis. Additionally, these results showcase the effectiveness and potential of our proposed method in tackling the challenges associated with multiple solutions in nonlinear differential equations with different types of boundary conditions.

1. Introduction

Nonlinear differential equations are widely used in various fields, and there are many versions of partial differential equations (PDEs) and ordinary differential equations (ODEs) available. One such example is reaction-diffusion equations, which find applications in physics, population dynamics, ecology, and biology. In physics, Simple kinetics, Belousov–Zhabotinskii reactions, and Low-temperature wave models are examples of applications. In population dynamics and ecology, the Prey-predator model and Pollution of the environment are relevant. In biology, reaction-diffusion equations are used to study Cell dynamics and Tumor growth [34]. Schrodinger equations [25] and Hamiltonian systems [24,33] are also important topics in the field of Quantum mechanics. Another important area in the realm of nonlinear PDEs is pattern formation, which has numerous applications, such as the Schnakenberg model [11], the Swift-Hohenberg equation [26], the Gray-Scott model [37], the FitzHugh-Nagumo equation [23], and the Monge–Ampère [14,16] equation, which finds various applications.

To solve these nonlinear PDEs and ODEs, various numerical methods have been developed, such as Newton's method and its variants, Min-Max method [36], bifurcation methods [45], multi-grid method [21,40] or subspace correction method [8] or a class of special two-grid methods [6,22,39–42], deflation method [13], mountain pass method [5,9], homotopy methods [17–19,35], Spectral methods [15], and using index-k saddle points [43,44]. However, finding multiple solutions remains a challenging task, primarily due to the difficulty of obtaining suitable initial guesses for each solution. Uncertainty often surrounds the existence of good numerical initial guesses that can reliably converge to these solutions. Even if such initial guesses exist, the process of finding them can be arduous and demanding.

To address this challenge, we introduce a novel approach called the Companion-Based Multilevel finite element method (CBMFEM) for solving nonlinear PDEs and ODEs using finite element methods with conforming elements. Our method is based on the structure of the full multigrid scheme [3] designed for the general nonlinear elliptic system. Given a coarse level, we compute a solution using a structured compan-

* Corresponding author.
E-mail addresses: wxh64@psu.edu (W. Hao), skl5876@psu.edu (S. Lee), yjlee@txstate.edu (Y.J. Lee).

https://doi.org/10.1016/j.camwa.2024.05.035
Received 23 August 2023; Received in revised form 6 May 2024; Accepted 31 May 2024

ion matrix, which is then transferred to the fine level to serve as an initial condition for the fine level. We use the Newton method to obtain the fine-level solution for each of these initial guesses and repeat this process until we obtain a set of solutions that converge to the stationary solutions of the PDEs and ODEs. Our approach distinguishes itself from existing literature, such as those presented in [5] or [28], where additional solutions are sought based on previously found solutions. By employing the CBMFEM, our goal is to efficiently and accurately identify multiple solutions for the specific class of elliptic semi-linear equations with polynomial nonlinear terms. While we focus on polynomial nonlinear terms in this paper, this particular case holds significant interest and potential, yet remains relatively unexplored.

The main advantage of our method is that it can generate multiple initial guesses efficiently and accurately, which is crucial for finding multiple solutions for nonlinear PDEs and ODEs. Furthermore, our method is robust and can be easily applied to a wide range of elliptic semi-linear equations with polynomial nonlinear terms.

As a theoretical foundation of CBMFEM, we present a mathematical definition of isolated solutions for elliptic semilinear PDEs and ODEs with multiple solutions, which leads to well-posedness of the discrete solution and provides a priori error estimates of the finite element solution using the framework introduced in [39].

We organize the paper as follows: In §2, we introduce the problem setup and basic assumptions. In §3, we summarize the error estimate of the nonlinear elliptic equation using the FEM method. In §4, we introduce the CBMFEM, including the construction of the companion matrix and filtering conditions. Finally, in §5, we present numerical results obtained using CBMFEM, which are consistent with the theoretical analysis. Throughout the paper, we use standard notation for Sobolev spaces $W^{k,p}(\Omega)$ and the norm $\|\cdot\|_{k,p}$. If $k=0$, then $\|\cdot\|_{0,p}$ denotes the L^p norm. The symbol $C^k(\Omega)$ denotes the space of functions, whose first $k \geq 0$ derivatives are continuous on Ω. Additionally, we denote $\underset{\sim}{v}$ as the vector while $\underset{\approx}{v}$ is the matrix.

2. Problem setup

We consider the following quasi-linear equation and assume that the polygonal (polyhedral) domain Ω is bounded in $\mathbb{R}^d$ with $d = 1, 2$, or 3:

$$-\Delta u + f(x,u) = 0, \quad \text{in } \Omega, \tag{1}$$

subject to the following general mixed boundary condition:

$$\alpha u + \beta \nabla u \cdot \mathbf{n} + \gamma g = 0, \quad \text{on } \partial\Omega. \tag{2}$$

Here $\mathbf{n}$ is the unit outward normal vector to $\partial\Omega$. The choices of α, β and γ impose the type of boundary conditions of u at $\partial\Omega$: Dirichlet boundary Γ_D, pure Neumann boundary Γ_N, mixed Dirichlet and Neumann boundary or the Robin boundary Γ_R, i.e.,

$$\partial\Omega = \overline{\Gamma}_D \cup \overline{\Gamma}_N \quad \text{or} \quad \partial\Omega = \overline{\Gamma}_R, \tag{3}$$

with $\overline{\Gamma}_D$, $\overline{\Gamma}_N$, and $\overline{\Gamma}_R$ being the closure of Γ_D, Γ_N, and Γ_R, respectively. Specifically,

$$\beta|_{\Gamma_D} = 0, \quad \alpha|_{\Gamma_N} = 0, \quad \text{and} \quad (\alpha\beta)|_{\Gamma_R} > 0. \tag{4}$$

We shall assume that g is smooth, and in particular when $\overline{\Gamma}_N = \partial\Omega$, compatibility conditions will be assumed for the functions f and g if necessary, [27]. For the sake of convenience, we denote $\Gamma_1 = \Gamma_R$ or Γ_N throughout this paper and assume that for some $c > 0$, a generic constant, the followings hold:

$$\beta = \gamma \quad \text{and} \quad 0 \leq \frac{\alpha}{\beta} \leq c \quad \text{on} \quad \Gamma_1. \tag{5}$$

We also provide some conditions for the function f, which is generally a nonlinear polynomial function in both x and u. We shall assume that $f(x,u) : \overline{\Omega} \times \mathbb{R} \mapsto \mathbb{R}$ is smooth in the second variable. We shall denote the k-th derivative of f with respect to u by $f^{(k)}$, i.e. $f^{(k)} = \frac{\partial^k f}{\partial u^k}$, and that there are positive constants C_1 and C_2 such that

$$|f(x,u)| \leq C_1 + C_2|u|^q, \tag{6}$$

where q is some real value, such that $1 \leq q \leq \infty$ for $d = 1$, $1 \leq q < \infty$ for $d = 2$ and $1 \leq q < 5$ for $d = 3$. This is sufficient for defining the weak formulation (see (8)). To apply the finite element method, we consider the weak formulation of Eq. (1) which satisfies the fully elliptic regularity (see [31] and references cited therein), i.e., solution is sufficiently smooth. We introduce a space V defined by:

$$V = \{v \in H^1(\Omega) : v|_{\Gamma_D} = 0\}. \tag{7}$$

The main problem can then be formulated as follows: Find $u \in V$ such that

$$\mathcal{F}(u,v) = a(u,v) + b(u,v) = 0, \quad \forall v \in V, \tag{8}$$

where $a(\cdot,\cdot), b(\cdot,\cdot) : V \times V \mapsto \mathbb{R}$ are the mappings defined as follows, respectively:

$$a(u,v) = \int_\Omega \nabla u \cdot \nabla v \, dx + \int_{\Gamma_1} \frac{\alpha}{\beta} uv \, ds, \quad \forall u, v \in V \tag{9a}$$

$$b(u,v) = \int_\Omega f(x,u)v \, dx + \int_{\Gamma_1} gv \, ds, \quad \forall u, v \in V. \tag{9b}$$

3. Finite element formulation and a priori error analysis

We will utilize a finite element method to solve (8), specifically a conforming finite element of degree $r \geq 1$. The triangulation of the domain Ω will be denoted by $\mathcal{T}_h = \{T\}_{i=1,\cdots,N_e}$. As usual, we define

$$h = \max_{T \in \mathcal{T}_h} \text{diam}(T). \tag{10}$$

Let V_h be the subspace of V that is composed of piecewise globally continuous polynomials of degree $r \geq 1$. We shall denote the dimension of V_h by N_h and

$$V_h = \text{span}\{\phi_h^i : i = 1, \cdots, N_h\}, \tag{11}$$

where ϕ_h^i is the basis of V_h. The discrete weak formulation for (8) is given as: Find $u_h \in V_h$ such that

$$\mathcal{F}(u_h, v_h) = a(u_h, v_h) + b(u_h, v_h) = 0, \quad \forall v_h \in V_h. \tag{12}$$

We note that for any $u_h \in V_h$, there exists a unique $\underset{\sim}{u}_h = (u_h^1, \cdots, u_h^{N_h})^T \in \mathbb{R}^{N_h}$ such that

$$u_h = \sum_{i=1}^{N_h} u_h^i \phi_h^i. \tag{13}$$

To obtain a solution u_h to (12), we need to solve the following system of nonlinear equations:

$$\underset{\sim}{F}_h(\underset{\sim}{u}_h) = \begin{pmatrix} F_h^1(\underset{\sim}{u}_h) \\ \vdots \\ F_h^{N_h}(\underset{\sim}{u}_h) \end{pmatrix} = \underset{\sim}{0}, \tag{14}$$

where

$$F_h^i(\underset{\sim}{u}_h) := a(u_h, \phi_h^i) + b(u_h, \phi_h^i) = 0, \quad \forall i = 1, \cdots, N_h. \tag{15}$$

3.1. A priori error analysis

In this section, we will discuss the convergence order of the finite element solutions for solving (8). Throughout this section, we introduce a notation for a fixed $\delta > 0$:

$$N_\delta = \{v \in V : \|u - v\|_{1,2} < \delta\}, \tag{16}$$

where u is a solution to the equation (8). We will make the following assumption:

Assumption 1. There exists a solution $u \in W^{1,\infty}(\Omega)$ of the problem (8) such that $\|u\|_{1,\infty} \le \Gamma$ for some constant Γ. Furthermore, in particular, u is isolated in the following sense: there exists $\delta = \delta_u > 0$ such that for all $w \in V$ such that $0 \neq \|w\|_{1,2} < \delta$, there exist $\eta_u > 0$ and $v_w \in V$, such that

$$\left|\mathcal{F}(u+w, v_w)\right| \ge \eta_u \|w\|_{1,2}\|v_w\|_{1,2} > 0. \tag{17}$$

Remark 1. We note that, to the best of our knowledge, this is the first time the notion of isolation has been adequately introduced in the literature. In [7], a similar definition is presented, but it allows v to be any function in V, not necessarily dependent on w in (17). This can lead to several critical issues. To illustrate one of the issues, we consider the problem of solving the following equation:

$$-u'' - u^p = 0 \quad \text{in} \quad \left(0, \frac{2\pi}{\sqrt{p}}\right) \subset \mathbb{R} \quad \text{subject to} \quad u(0) = u\left(\frac{2\pi}{\sqrt{p}}\right) = 0, \tag{18}$$

where $p > 0$. The weak form is given by $\mathcal{F}(u,v) = \int_\Omega \nabla u \cdot \nabla v dx - \int_\Omega u^p v dx = 0$ and $u = 0$ is an isolated solution in the sense of (17), namely, for any $w \in V$, we choose $v_w = w$, so that we have

$$|\mathcal{F}(u+\varepsilon w, w)| = \left| \int_\Omega \nabla(\varepsilon w)\cdot \nabla w - \varepsilon^p \int_\Omega w^{p+1} \right| \ge \eta_u \|\varepsilon w\|_{1,2}\|w\|_{1,2}, \tag{19}$$

for some η_u, no matter how ε is small, due to the Sobolev embedding, i.e., $\|w\|_{0,p+1} \lesssim \|w\|_{1,2}$. On the other hand, if we choose $w = \cos(\sqrt{p}x) - 1$, $0 < \varepsilon \ll 1$ and $v = \sin(\sqrt{p}x)$, then we have that

$$\mathcal{F}(u+\varepsilon w, v) = \varepsilon \int_\Omega \nabla w \cdot \nabla v dx - \varepsilon^p \int_\Omega w^p v dx = -\varepsilon^p \int_\Omega w^p v dx = 0, \tag{20}$$

which implies that $0 = |\mathcal{F}(u+\varepsilon w, v)| \ge \eta_u \varepsilon \|w\|_{1,2}\|v\|_{1,2} = O(\varepsilon)$. This does not make sense.

We begin with the following lemma as a consequence of our assumption:

Lemma 1. *Under the assumption that $\|u\|_{0,\infty} \le \Gamma$, we have*

$$\|f^{(1)}\|_{0,\infty}, \|f^{(2)}\|_{0,\infty} < C(\Gamma), \tag{21}$$

where C is a constant that depends on Γ.

We shall now consider the linearized problem for a given isolated solution u to the equation (8): For $q \in V^*$, find $w \in V$ such that

$$A(u; w, v) := a(w,v) + \int_\Omega f^{(1)}(u) w v \, dx = (q, v), \quad \forall v \in V. \tag{22}$$

We shall now establish the well-posedness of the linearized problem as follows.

Lemma 2. *$A(u;\cdot,\cdot)$, defined in Eq. (22), satisfies the inf-sup condition, i.e.,*

$$\inf_{w\in V}\sup_{v\in V} \frac{A(u;v,w)}{\|v\|_{1,2}\|w\|_{1,2}} = \inf_{v\in V}\sup_{w\in V} \frac{A(u;v,w)}{\|v\|_{1,2}\|w\|_{1,2}} \gtrsim 1. \tag{23}$$

Proof. Based on [1], we need to prove that

(i) there exists a unique zero solution, $w = 0$, to $A(u;w,v) = 0$ for all $v \in V$;

(ii) $A(u;\cdot,\cdot)$ satisfies the Garding-type inequality, i.e., there exist $\gamma_0, \gamma_1 > 0$ such that

$$|A(u;v,v)| \ge \gamma_0 \|v\|_{1,2}^2 - \gamma_1 \|v\|_{0,2}^2, \quad \forall v \in V,$$

For the second condition, the Garding-type inequality holds due to the Poincare inequality [12]. Secondly, we will prove the first condition using the proof by contradiction. Let us assume that there exists a non-zero solution $w \in V$ such that

$$A(u;w,v) = 0, \quad \forall v \in V. \tag{24}$$

Then, for ϵ sufficiently small, we define $u_\epsilon = u + \epsilon w \in N_\delta(u)$. Then, by Assumption 1, we can choose $v_w \in V$, for which the inequality (17) holds and observe that

$$\begin{aligned}
&\mathcal{F}(u+\epsilon w, v_w)\\
&= a(u+\epsilon w, v_w) + b(u+\epsilon w, v_w) = a(u+\epsilon w, v_w)\\
&\quad + \int_\Omega \left[f(u) + f^{(1)}(u)(\epsilon w) + \frac{1}{2} f^{(2)}(\xi)(\epsilon w)^2\right] v_w \, dx - \int_{\Gamma_{D_c}} g v_w \, ds\\
&= a(u, v_w) + b(u, v_w) + A(u, \epsilon w, v_w) + \frac{1}{2}\epsilon^2 \int_\Omega f^{(2)}(\xi) w^2 v_w \, dx\\
&\le \frac{\epsilon^2}{2} \|f^{(2)}\|_{0,p_1} \|w\|_{0,2p_2}^2 \|v_w\|_{0,p_3},
\end{aligned}$$

where the last inequality used the generalized Hölder inequality with p_i for $i = 1,2,3$, satisfying the identity $\frac{1}{p_1} + \frac{1}{p_2} + \frac{1}{p_3} = 1$. Since we can choose ϵ to be arbitrarily small, this contradicts Assumption 1. Thus, the proof is complete. □

We note that the equation (22) corresponds to the following partial differential equation: find w such that

$$-\Delta w + f^{(1)}(u) w = q \quad \text{in } \Omega, \tag{25}$$

subject to the same type of boundary condition to the equation (8), but with g replaced by zero function in (2). We shall assume that the solution to the equation (22) satisfies the full elliptic regularity, i.e.,

$$\|w\|_{2,p_0} \lesssim \|q\|_{0,2}, \tag{26}$$

with $p_0 = 2$. The assumption holds true for the convex domain under both Dirichlet and pure Neumann boundary conditions. However, for the mixed boundary case, it is valid for certain values of $p_0 > 4/3$ (see [10], Corollary 3.12). Of course, an assumption can be relaxed to $p_0 < 2$, which then, as a result induces a complexity in the presentation.

After establishing the inf-sup condition for the linearized equation at the continuous level, we can establish the discrete inf-sup condition using the standard techniques such as the $W^{1,2}$ stability and L^2 norm error estimate of Ritz-projection for sufficiently small h (see [4,27]).

Lemma 3. *Under the Assumption 1, the following discrete inf-sup condition holds if $h < h_0$ for sufficiently small h_0. Specifically, there exists α_0, which is independent of h, such that*

$$\inf_{w_h\in V_h}\sup_{v_h\in V_h} \frac{A(u;v_h,w_h)}{\|v_h\|_{1,2}\|w_h\|_{1,2}} = \inf_{v_h\in V_h}\sup_{w_h\in V_h} \frac{A(u;v_h,w_h)}{\|v_h\|_{1,2}\|w_h\|_{1,2}} = \alpha_0 > 0. \tag{27}$$

This finding has implications for the well-posedness of the Newton method used to find solutions. For a more in-depth discussion of using the Newton method to find multiple solutions, see [29,30,36] and the references cited therein. We shall now consider the solution operator for $A(u;\cdot,\cdot)$ and the error estimates. First we define the projection operator $\pi_h : V \mapsto V_h$ as

$$A(u;\pi_h w, v_h) = A(u; w, v_h), \quad \forall v_h \in V_h. \tag{28}$$

Lemma 4. *For the projection operator, we have with $r \geq 1$,*

$$\|w - \pi_h w\|_{0,2} \lesssim h^{r+1}\|w\|_{r+1,2} \quad \text{and} \quad \|w - \pi_h w\|_{1,2} \lesssim h^r \|w\|_{r+1,2}. \tag{29}$$

The following inequality shall be needed for the well-posedness and error analysis of the discrete solution, which is well-known to be true, for the Dirichlet boundary condition case (see Theorem 7.1.11 and §7.5 in [4]), it is shown to hold:

$$\|\pi_h v\|_{0,\infty} \lesssim \|v\|_{1,\infty}, \quad \forall v \in W^{1,\infty}(\Omega), \quad \text{for } h < h_0, \tag{30}$$

where h_0 is sufficiently small. For the mixed boundary condition, it is unclear yet, if such an estimate holds (see [27] for example for a special 2D case), which is beyond the scope to deal with in this paper. We shall now present the result that the discrete problem (12) admits a unique solution u_h that can approximate the fixed isolated solution u with the desired convergence rate in both L^2 and $W^{1,2}$ norm, using the argument employed in [40].

Theorem 3.1. *Suppose the Assumption 1 and (30). Then, for $0 < h < h_0$, with h_0 sufficiently small, the finite element equation (12) admits an isolated solution u_h satisfying*

$$\|u - u_h\|_{k,2} \lesssim h^{r+1-k}, \quad \text{for } k = 0, 1. \tag{31}$$

Furthermore, u_h is the only solution in N_δ for some $\delta > 0$ such that $\|u_h\|_{0,\infty} \leq \Gamma_1$ for some generic Γ_1.

Proof. We first note that for any $v, v_h, \chi \in V$, it holds

$$\mathcal{F}(v_h, \chi) = \mathcal{F}(v, \chi) + A(v; v_h - v, \chi) + R(v, v_h, \chi), \tag{32}$$

where $R(v, v_h, \chi) = \int_\Omega [f(v_h) - f(v) - f^{(1)}(v)(v_h - v)]\chi \, dx$. We now define a nonlinear operator $\Phi : V_h \to V_h$ by

$$A(u; \Phi(v_h), v_h) = A(u; u, v_h) - R(u, v_h, v_h), \quad \forall v_h \in V_h.$$

Then, from the inf-sup condition, Φ is well-defined. We shall invoke the Brower Fixed point theorem for the mapping Φ and thus, we introduce a closed ball of the space V_h defined as follows:

$$B = \{v \in V_h : \|v - \pi_h u\|_{1,2} \leq 2C_0 h^r \text{ and } \|v\|_{0,\infty} \leq \Gamma_0 + 1\},$$

where C_0 and Γ_0 are generic constants. Using the inverse-type inequality (see Lemma 4.5.3 in [4]), we can show that the ball B is closed in V. Furthermore, from the Lemma 1, the mapping Φ is continuous on B. We shall now show that Φ is a mapping from B to B. Using the mean-value theorem, we observe that the following inequality holds for $v_h \in B$ and $\chi \in V$,

$$\begin{aligned} A(u; \Phi(v_h) - \pi_h u, \chi) &= A(u; u - \pi_h u, \chi) - R(u, v_h, \chi) \\ &\lesssim \|u - \pi_h u\|_{1,2}\|\chi\|_{1,2} + \int_\Omega |u - v_h|^2 |\chi| \, dx. \end{aligned}$$

By applying the Cauchy-Schwarz inequality and the Sobolev embedding theorem, we obtain the following inequality (with $1/p + 1/q = 1$),

$$\begin{aligned} \int_\Omega (u - v_h)^2 |\chi| \, dx &\lesssim \left(\int_\Omega |u - v_h|^{2p} \, dx \right)^{1/p} \left(\int_\Omega |\chi|^q \, dx \right)^{1/q} \\ &\lesssim \|u - v_h\|_{0,2}^{1+\epsilon} \|\chi\|_{0,q} \lesssim \|u - v_h\|_{0,2}^{1+\epsilon} \|\chi\|_{1,2}, \end{aligned}$$

for some $0 < \epsilon \leq 1$ for $d = 1, 2$ or $d = 3$. More precisely, for $d = 1$, we can choose $p = 1$ and $q = \infty$, thus $\epsilon = 1$. On the other hand, for $d = 2$ and $d = 3$, we can set $q = 6$ and $p = 6/5$, then $\epsilon = 2/3$, both by the assumption that $\|u\|_{1,\infty} \leq \Gamma$ and that Ω is a bounded domain. By using the Garding's inequality, we obtain the following inequality:

$$\|\chi\|_{1,2}^2 - \|\chi\|_{0,2}^2 \lesssim |A(u; \chi, \chi)| \lesssim C_1 h^r \|\chi\|_{1,2} + \|u - v_h\|_{0,2}^{1+\epsilon} \|\chi\|_{1,2}, \quad \forall \chi \in V.$$

Thus, since $\|\chi\|_{0,2} \leq \|\chi\|_{1,2}$, we have

$$\|\chi\|_{1,2} \lesssim \|\chi\|_{0,2} + \|u - v_h\|_{0,2}^{1+\epsilon} + C_1 h^r. \tag{33}$$

Next, we consider the duality argument for the linearized equation that for a given $q \in V^*$ as follows with $\chi = \Phi(v_h) - \pi_h u \in V_h$:

$$\begin{aligned} (\chi, q) = A(u; \chi, w) &= A(u; \chi, w - \Pi_h w) + A(u; \chi, \Pi_h w) \\ &\lesssim \|\chi\|_{1,2}\|w - \Pi_h w\|_{1,2} + \|u - v_h\|_{0,2}^{1+\epsilon}\|\Pi_h w\|_{1,2} \\ &\lesssim h\|\chi\|_{1,2}\|w\|_{2,2} + \|u - v_h\|_{0,2}^{1+\epsilon}\|\Pi_h w\|_{1,2} \\ &\lesssim h\|\chi\|_{1,2}\|q\|_{0,2} + \|u - v_h\|_{0,2}^{1+\epsilon}\|w\|_{2,2} \\ &= (h\|\chi\|_{1,2} + \|u - v_h\|_{0,2}^{1+\epsilon})\|q\|_{0,2}, \end{aligned}$$

where we used the assumption on the full elliptic regularity (26) and property of Scott-Zhang interpolation [32]. By setting $q = \chi$, we arrive at

$$\|\chi\|_{0,2} \lesssim h\|\chi\|_{1,2} + \|u - v_h\|_{0,2}^{1+\epsilon}. \tag{34}$$

Therefore, we have that

$$\|\chi\|_{1,2} \lesssim h\|\chi\|_{1,2} + 2\|u - v_h\|_{0,2}^{1+\epsilon} + C_1 h^r. \tag{35}$$

On the other hand, we have that

$$\|u - v_h\|_{0,2}^{1+\epsilon} \leq \|u - \pi_h u\|_{0,2}^{1+\epsilon} + \|v_h - \pi_h u\|_{0,2}^{1+\epsilon} = o(1)h^r. \tag{36}$$

Therefore, for $h < h_0$ sufficiently small, we arrive at for all $v_h \in B$

$$\|\Phi(v_h) - \pi_h u\|_{1,2} \leq 2C_0 h^r. \tag{37}$$

Lastly, we notice that by the inverse inequality (see Theorem 4.5.11 in [4]), there exists $\sigma > 0$ such that

$$\|\Phi(v_h) - \pi_h u\|_{0,\infty}^2 \lesssim \ell(h)\|\Phi(v_h) - \pi_h u\|_{1,2}^2 \leq \ell(h) h^{2r} \lesssim h^\sigma,$$

where $\ell(h) = 1$ for $1D$ and $|\log h|^2$ for $2D$ and h^{-1} for $3D$. Now, we invoke the condition (30) to arrive at $\Phi(B) \subset B$. Thus, the Brouwer's fixed point theorem shows the existence of $u_h \in B$ such that $\Phi(u_h) = u_h$. The uniqueness can follow from the inf-sup condition (27) and the continuity of the isormophic operator as a function of the point where the linearization is made, as discussed in [40]. To obtain the L^2 estimate, we use the fact that $\|u - u_h\|_{1,2} \lesssim h^r$ resulting from the above argument. We then replace v_h by u_h in the inequality (34) and we are led to the following inequality:

$$\|u - u_h\|_{0,2} \lesssim h^{r+1} + \|u - u_h\|_{0,2}^{1+\epsilon}, \tag{38}$$

where $0 < \epsilon \leq 1$. Thus, by the Kick-Back argument, we arrive at the conclusion. This completes the proof. □

4. Companion-based multilevel finite element method (CBMFEM)

In this section, we present a companion-based multilevel finite element method to solve the nonlinear system (14). Solving this system directly is challenging due to the presence of multiple solutions. Therefore, we draw inspiration from the multigrid method discussed in [3] that is designed for a single solution. We modify the multilevel finite element method by introducing a local nonlinear solver that computes the eigenvalues of the companion matrix. This enables us to generate a set of initial guesses for Newton's method, which is used to solve the nonlinear system on the refined mesh.

We begin by introducing a sequence of nested triangulations, namely,

$$\mathcal{T}_0, \mathcal{T}_1, \mathcal{T}_2, \cdots, \mathcal{T}_N, \tag{39}$$

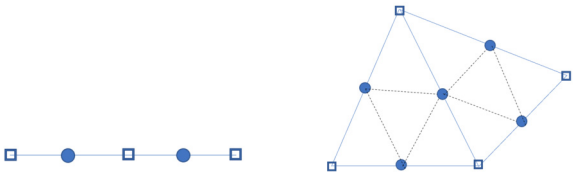

Fig. 1. Mesh refinement of CBMFEM in 1D (left) and 2D with edge (right). The square dots are the coarse nodes while filled circles are newly introduced fine nodes.

where $\mathcal{T}_0$ and $\mathcal{T}_N$ are the coarsest and the finest triangulations of Ω, respectively. This leads to the construction of a sequence of nested and conforming finite element spaces $\{V_\ell\}_{\ell=0}^{N} \subset V$, given as follows:

$$V_0 \subset \cdots \subset V_N. \tag{40}$$

The refinement strategy is shown in Fig. 1 for both 1D and 2D cases, where we introduce new nodes (the filled circles) based on the coarse nodes (the square dots). Specifically, for a given coarse mesh $\mathcal{T}_H$, we obtain the refined mesh $\mathcal{T}_h$ by introducing a new node on $\mathcal{V}_H$. The overall flowchart of CBMFEM is summarized in Fig. 2.

Assuming that a solution $u_H \in V_H$ on a coarse mesh $\mathcal{T}_H$ has been well approximated, namely $\underset{\sim}{F}_H(\underset{\sim}{u}_H) = \underset{\sim}{0}$, we can refine the triangulation $\mathcal{T}_H$ to obtain a finer triangulation $\mathcal{T}_h$. Since $\mathcal{V}_H \subset \mathcal{V}_h$, we can find a function $\widetilde{u}_h(x)$ in $\mathcal{V}_h$ such that we can express $u_H(x)$ as a linear combination of the basis functions of $\mathcal{V}_h$:

$$u_H(x) = \widetilde{u}_h(x) = \sum_{i=1}^{\dim \mathcal{V}_h} \widetilde{u}_h^i \phi_h^i(x), \tag{41}$$

where $\dim \mathcal{V}_h$ is the dimension of $\mathcal{V}_h$ and $\phi_h^i(x)$ are the basis functions of $\mathcal{V}_h$. In particular, for any point $x_i \in \mathcal{V}_H$, we have $\widetilde{u}_h^i = u_H(x_i)$. For points $x_i \in \mathcal{V}_h \backslash \mathcal{V}_H$, we can calculate $\widetilde{u}_h^i$ based on the intrinsic structure of the basis functions. In other words, we can interpolate $u_H(x)$ to $u_h(x)$ by using the basis functions on two levels. Specifically, let's consider 1D case and have the relation $\phi_H^{i/2} = \phi_{2h}^{i/2} = \frac{\phi_h^{i-1}}{2} + \phi_h^i + \frac{\phi_h^{i+1}}{2}$, which allows us to calculate the coefficients for (41). More precisely, we can write $u_H(x)$ to $u_h(x)$ as follows:

$$\begin{aligned} u_H(x) &= \sum_{x_i \in V_H} u_H^{i/2} \phi_H^{i/2}(x) = \sum_{x_i \in V_H} u_H^{i/2} \left(\frac{\phi_h^{i-1}}{2} + \phi_h^i + \frac{\phi_h^{i+1}}{2} \right) \\ &= \sum_{i=1}^{\dim \mathcal{V}_h} \widetilde{u}_h^i \phi_h^i(x). \end{aligned} \tag{42}$$

We next update the value of u_h^i for $x_i \in \mathcal{V}_h \backslash \mathcal{V}_H$ on the fine mesh. To do this, we solve $F_h^i(u_h^i; (u_h^j = \widetilde{u}_h^j)_{j \neq i}) = 0$ for u_h^i by fixing the values of other nodes as $\widetilde{u}_h$. Since $f(x,u)$ is a polynomial, we can rewrite F_h^i as a single polynomial equation, namely,

$$F_h^i(u_h^i; (u_h^j = \widetilde{u}_h^j)_{j \neq i}) = P_h^i(\widehat{u}_h^i) = 0, \tag{43}$$

where $P_h^i(\alpha) = \sum_{n=0}^{m} c_n \alpha^n$. The companion matrix of $P_h^i(\alpha)$ is defined as

$$C(P_h^i) = \begin{bmatrix} 0 & 0 & \dots & 0 & -c_0/c_m \\ 1 & 0 & \dots & 0 & -c_1/c_m \\ 0 & 1 & \dots & 0 & -c_2/c_m \\ \vdots & \vdots & \ddots & \vdots & \vdots \\ 0 & 0 & \dots & 1 & -c_{m-1}/c_m \end{bmatrix}, \tag{44}$$

where, except for c_0, the coefficients c_n depend only on $\{\widetilde{u}_h^j\}$ that are near the point $x_i \in \mathcal{V}_h \backslash \mathcal{V}_H$, making their computation local. By denoting the root of Eq. (43) as $\widehat{u}_h^i$, the initial guess for the solutions on V_h is set as

$$\widehat{u}_h = \sum \widehat{u}_h^i \phi_h^i \text{ where } \widehat{u}_h^i = \begin{cases} u_H^i, & x_i \in \mathcal{V}_H, \\ \widehat{u}_h^i \text{ by solving (43)}, & x_i \in \mathcal{V}_h \backslash \mathcal{V}_H. \end{cases} \tag{45}$$

Since all the eigenvalues of $C(P_h^i)$ satisfy the equation $P_h^i(y_i) = 0$, there can be up to $m^{|\mathcal{V}_h \backslash \mathcal{V}_H|}$ possible initial guesses, where $|\mathcal{V}_h \backslash \mathcal{V}_H|$ denotes the number of newly introduced fine nodes on $\mathcal{V}_h$ and m is the degree of the polynomial (43). However, computing all of these possibilities is computationally expensive, so we apply the filtering conditions below to reduce the number of initial guesses and speed up the method:

- **Locality condition:** we assume the initial guess is near $\underset{\sim}{\tilde{u}}_h$ in term of the residual, namely,

$$\| \underset{\sim}{F}_h(\underset{\sim}{\widehat{u}}_h) \|_{0,2} < C_1 \| \underset{\sim}{F}_h(\underset{\sim}{\tilde{u}}_h) \|_{0,2}; \tag{46}$$

- **Convergence condition:** we apply the convergence estimate to the initial guess, namely,

$$\| \underset{\sim}{F}_h(\underset{\sim}{\widehat{u}}_h) \|_{0,2} < C_2 h^2; \tag{47}$$

- **Boundness condition:** we assume the initial guess is bounded, namely,

$$\| \underset{\sim}{\widehat{u}}_h \|_{0,\infty} < C_3. \tag{48}$$

Finally, we summarize the algorithm of CBMFEM in **Algorithm 1**.

Algorithm 1 CBMFEM for computing multiple solutions.

Given V_h, V_H, and solution u_H on V_H.
  Interpolate $u_H = \sum \widetilde{u}_h^i \phi_h^i$ and compute coefficient $\widetilde{u}_h^i$.
  for $i \in V_h \backslash V_H$ **do**
    Construct the polynomial equation $P_h^i(\widehat{u}_h^i)$
    Compute the eigenvalues of the companion matrix, $C(P_h^i)$
  end for
  Obtain initial guesses in (45) on V_h and apply filtering conditions.
  Employ Newton method on V_h with the obtained initial guesses to solve $\underset{\sim}{F}_h(\underset{\sim}{u}_h) = 0$

5. Numerical examples

In this section, we present several examples for both 1D and 2D to demonstrate the effectivity and robustness of CBMFEM with $r = 1$ for simplicity. We shall let $e_H^h = u_h - u_H$ where u_h and u_H are the numerical solutions with grid step size h and H, respectively, and u is the analytical solution. For error analysis, since most of the examples we considered do not have analytical solutions, we used asymptotic error analysis to calculate the convergence rate.

5.1. Examples for 1D

5.1.1. Example 1

First, we consider the following boundary value problem

$$\begin{cases} -u'' - (1 + u^4) = 0, & \text{in} \quad (0,1), \\ u'(0) = u(1) = 0, \end{cases} \tag{49}$$

which has analytical solutions [17]. More specifically, by multiplying both sides with u' and integrating with respect to x, we obtain

$$\frac{(u'(x))^2}{2} + F(u(x)) - F(u_0) = 0, \tag{50}$$

where $F(u) = u + \frac{u^5}{5}$ and $u_0 = u(0)$. Since $u'(0) = 0$ and $u''(x) < 0$, then we have $u' < 0$ for all $x > 0$. Moreover, $u(x) < u_0$ implies $F(u_0) > F(x)$ for all $x > 0$. Therefore

$$\frac{u'(x)}{\sqrt{F(u_0) - F(u(x))}} = -\sqrt{2}. \tag{51}$$

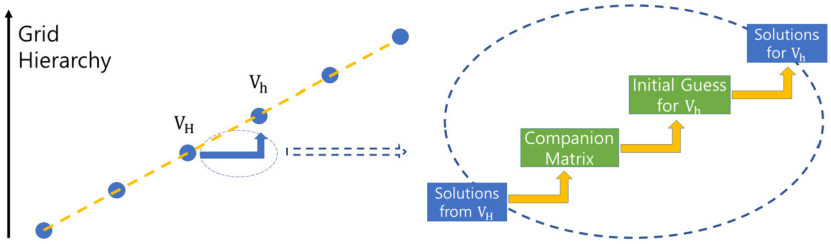

Fig. 2. A flowchart of the CBMFEM for solving the nonlinear differential equation. The hierarchical structure of CBMFEM is illustrated on the left, where for each level, we obtain a solution on the coarse grid, V_H. We then solve local nonlinear equations by constructing companion matrices and generate initial guesses for Newton's method on the finer level V_h on the right.

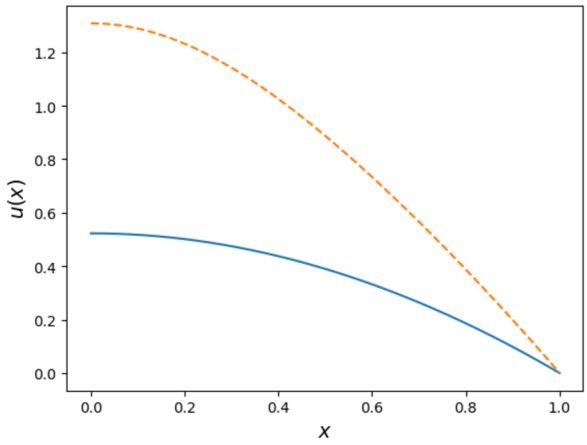

Fig. 3. Numerical solutions of Eq. (49) with $N = 1025$ grid points. The unstable solution is plotted with dashed lines, while the stable solution is represented with solid lines.

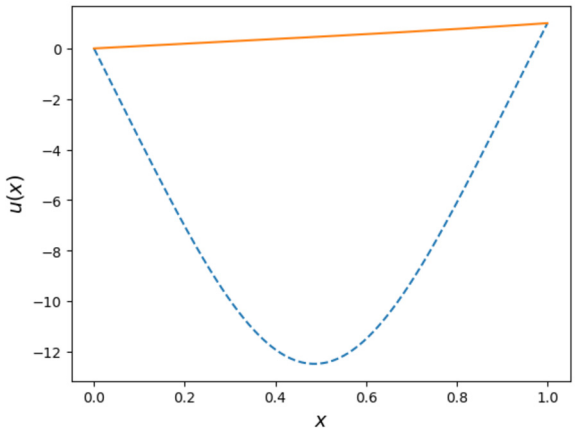

Fig. 4. Numerical solutions of Eq. (56) with $N = 1025$ grid points. The unstable solution is plotted with dashed lines, while the stable solution is represented with solid lines.

By integrating x from s to 1, we obtain

$$\int_s^1 \frac{u'(x)}{\sqrt{F(u_0) - F(u(x))}} dx = -\sqrt{2}(1-s). \tag{52}$$

Due to the boundary condition $u(1) = 0$, we have

$$\int_0^{u(s)} \frac{du}{\sqrt{F(u_0) - F(u)}} = \sqrt{2}(1-s). \tag{53}$$

By choosing $s = 0$, we have the following equation for u_0,

$$\int_0^{u_0} \frac{du}{\sqrt{F(u_0) - F(u)}} = \sqrt{2} \tag{54}$$

Then for any given u_0, the solution of (49) is uniquely determined by the initial value problem

$$\begin{cases} -v' = (1+u^4) \\ u' = v \end{cases} \quad \text{with} \quad \begin{cases} v(0) = 0 \\ u(0) = u_0 \end{cases}. \tag{55}$$

By solving (54) with Newton's method, we get two solutions $u_0 \approx 0.5227$ and $u_0 \approx 1.3084$. Then the numerical error is shown in Table 1 for the CBMEFM with Newton's nonlinear solver. The solutions with $N = 1025$ grid points are shown in Fig. 3. The unstable solution is plotted with dashed lines, while the stable solution is represented with solid lines. We additionally compare our method with the traditional homotopy method, as detailed in Table 2. CBMFEM achieves computing times of less than 1 second for the coarse grids up to $N = 17$, whereas the homotopy method can only handle the coarse grids up to $N = 12$, requiring over 1 hour due to its significant computational overhead [2].

5.1.2. Example 2

Next, we consider the following boundary value problem

$$\begin{cases} -u'' + u^2 = 0, \quad \text{in} \quad (0,1), \\ u(0) = 0 \text{ and } u(1) = 1, \end{cases} \tag{56}$$

which has two solutions shown in Fig. 4. We start $N = 3$ and compute the solutions up to $N = 1025$ by implementing CBMEFM with a nonlinear solver. We compute the numerical error by using $\|e_H^h\|_{0,2}$ and summarize the convergence test and computing time in Table 3. We also compare our method with the traditional homotopy method, as detailed in Table 4. CBMFEM is much more efficient than the homotopy method on the coarse grids up to $N = 17$ [2].

5.1.3. Example 3

Thirdly, we consider the following nonlinear parametric differential equation

$$\begin{cases} -u'' - u^2(p - u^2) = 0 \quad \text{in} \quad (0,1), \\ u'(0) = u(1) = 0, \end{cases} \tag{57}$$

where p is a parameter. The number of solutions increases as p gets larger [20]. We compute the numerical solutions for $p = 1, 7$, and 18 using CBMEFM with Newton's solver and show the solutions in Fig. 5. The computation time and the number of solutions for different values of p and step sizes are summarized in Table 5. As p increases, the number of solutions increases, and hence the computation time becomes longer. Numerical error and convergence order are shown in Table 6.

5.1.4. Example 4

We consider the following semi-linear elliptic boundary value problem

Table 1
Numerical errors and computing time of CBMEFM with Newton's nonlinear solver for solving Eq. (49).

h	# 1st Solution				# 2nd solution				CPU(s)
	$\|e_h\|_{0,2}$	Order	$\|e_h\|_{1,2}$	Order	$\|e_h\|_{0,2}$	Order	$\|e_h\|_{1,2}$	Order	Newton
2^{-2}	2.6E-04	x	1.7E-01	x	8.3E-03	x	7.0E-02	x	0.10
2^{-3}	6.4E-05	2.01	8.0E-02	1.00	2.0E-03	2.04	4.0E-02	1.01	0.10
2^{-4}	1.6E-05	2.00	4.0E-02	1.00	5.0E-04	2.01	2.0E-02	1.00	0.15
2^{-5}	4.0E-06	2.00	2.0E-02	1.00	1.3E-04	2.00	9.3E-03	1.00	0.16
2^{-6}	1.0E-06	2.00	1.0E-02	1.00	3.1E-05	2.00	4.7E-03	1.00	0.11
2^{-7}	2.5E-07	2.00	5.2E-03	1.00	7.8E-06	2.00	2.3E-03	1.00	0.16
2^{-8}	6.2E-08	2.00	2.6E-03	1.01	1.9E-06	2.00	1.2E-03	1.01	0.25
2^{-9}	1.6E-08	2.00	1.3E-03	1.03	4.9E-07	2.00	0.6E-03	1.04	0.64
2^{-10}	3.9E-09	2.00	5.6E-04	1.16	1.2E-07	2.00	0.3E-03	1.16	3.55

Table 2
Computing time of homotopy method and CBMFEM vs. Number of Grid Points, N on **Example 1**. Both methods can find two solutions for this example. For the homotopy method, Bertini was employed for implementation [2]. However, due to the large computational cost, computations were not performed for $N \geq 12$ as they were estimated to exceed 5 hours. For CBMFEM, computations were conducted for $N = 2^{\ell} + 1$ where $\ell = 0, \cdots, 4$.

N \ CPU time in sec	Homotopy Method	CBMFEM
3	0.008 s	0.03 s
4	0.02 s	N/A
5	0.059 s	0.10 s
6	0.295 s	N/A
7	1.624 s	N/A
8	8.261 s	N/A
9	50.278 s	0.10 s
10	231.353 s	N/A
11	916.459 s	N/A
12	4506.12 s	N/A
13	N/A	N/A
14	N/A	N/A
15	N/A	N/A
16	N/A	N/A
17	N/A	0.15 s

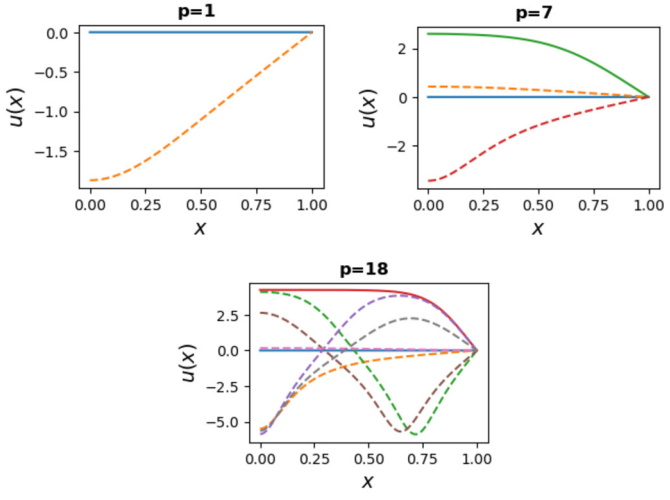

Fig. 5. Numerical solutions of Eq. (57) with 1025 grid points for $p = 1$, $p = 7$, and $p = 18$, respectively. Unstable solutions are plotted with dashed lines, while stable solutions are represented with solid lines.

$$\begin{cases} -u''(x) - d^{r+2}|x|^r u^3(x) = 0 \quad \text{in} \quad (-1,1), \\ u(-1) = u(1) = 0, \end{cases} \tag{58}$$

where d is the scaling coefficient corresponding to the domain. This example is based on a problem considered in [38]. We have re-scaled the domain from $(-1,1)$ to $(-d,d)$ and formulated the problem accordingly.

We start with $r = 3$ and $d = 1$ and find 4 non-negative solutions with $N = 1025$ using CBMEFM. The numerical error and convergence order are shown in Table 7. Using the homotopy method with respect to both r and d, we also discover the same number of solutions for $r = 3, d = 10$ and $r = 12, d = 1$. The numerical solutions with different parameters are shown in Fig. 6. Then, we also create a bifurcation diagram for the numerical solutions with respect to r by choosing $d = 1$ and using 1025 grid points, as shown in Fig. 7. We only display the non-trivial non-negative solutions on this diagram. When r is small, we have only one non-trivial solution. As r increases, the number of non-trivial solutions increases and bifurcates to three solutions.

5.1.5. The Schnakenberg model

We consider the steady-state system of the Schnakenberg model in 1D with no-flux boundary conditions

$$\begin{cases} -u'' - \eta(a - u + u^2 v) = 0, \quad \text{in} \quad (0,1) \\ -dv'' - \eta(b - u^2 v) = 0, \quad \text{in} \quad (0,1) \\ u'(0) = u'(1) = v'(0) = v'(1) = 0. \end{cases} \tag{59}$$

This model exhibits complex solution patterns for different parameters η, a, b, and d [19]. In [19], the homotopy continuation method was used. The results are reproduced using CBMFEM. Since there is only one nonlinear term $u^2 v$, we rewrite the steady-state system as follows

$$\begin{cases} -u'' - dv'' - \eta(a + b - u) = 0, \\ -dv'' - \eta(b - u^2 v) = 0. \end{cases} \tag{60}$$

In this case, we only have one nonlinear equation in the system (60). After discretization, we can solve $\underset{\sim}{v}_h$ in terms of $\underset{\sim}{u}_h$ using the first equation and plug it into the second equation. We obtain a single polynomial equation of $\underset{\sim}{u}_h$, which allows us to use the companion matrix to solve for the roots. Then we use CBMEFM to solve the Schakenberg model in 1D with the parameters $a = 1/3, b = 2/3, d = 50, \eta = 50$ up to $h = 2^{-9}$. There are 3 solutions computed Fig. 8 and we show the computing time in Table 8.

5.2. Examples in 2D

In this section, we discuss a couple of two dimensional examples.

5.2.1. Example 1

$$\begin{cases} -\Delta u(x,y) - u^2(x,y) = -s\sin(\pi x)\sin(\pi y) \quad \text{in} \quad \Omega, \\ u(x,y) = 0, \quad \text{in} \quad \partial\Omega \end{cases} \tag{61}$$

where $\Omega = (0,1) \times (0,1)$ [5]. In [5], the numerical Mountain pass algorithm was used. The results are reproduced using CBMFEM.

In this example, we utilized edge refinement to generate a multi-level grid and provide multiple initial guesses for the next level, as shown in Fig. 9. The number of nodes and triangles on each level is summarized in Table 9.

First, we compute the solutions with $s = 1600$. We only applied the CBMEFM for the first three multi-level grids until $\ell = 2$ due to the ex-

Table 3
Numerical errors and computing time of CBMEFM with Newton's solver for solving Eq. (56).

h	# 1st solution				# 2nd solution				CPUs
	$\|e_H^h\|_{0,2}$	Order	$\|e_H^h\|_{1,2}$	Order	$\|e_H^h\|_{0,2}$	Order	$\|e_H^h\|_{1,2}$	Order	Newton
2^{-2}	2.6E-3	x	2.3E-2	x	7.9E-1	x	5.8E-0	x	0.09
2^{-3}	6.8E-4	1.96	1.2E-2	0.90	2.0E-1	2.01	2.9E-0	1.03	0.09
2^{-4}	1.7E-4	1.99	6.3E-3	0.94	4.9E-2	2.00	1.4E-0	1.00	0.09
2^{-5}	4.3E-5	2.00	3.2E-3	0.97	1.2E-2	2.00	7.12E-1	1.00	0.10
2^{-6}	1.1E-5	2.00	1.6E-3	0.98	3.1E-3	2.00	3.6E-1	1.00	0.11
2^{-7}	2.7E-6	2.00	8.2E-4	0.99	7.7E-4	2.00	1.8E-1	1.00	0.14
2^{-8}	6.7E-7	2.00	4.1E-4	1.00	1.9E-4	2.00	8.9E-2	1.00	0.24
2^{-9}	1.7E-7	2.00	2.1E-4	1.00	4.8E-5	2.00	4.5E-2	1.00	0.49
2^{-10}	4.2E-8	2.00	1.0E-4	1.00	1.2E-5	2.00	2.2E-2	1.00	3.35

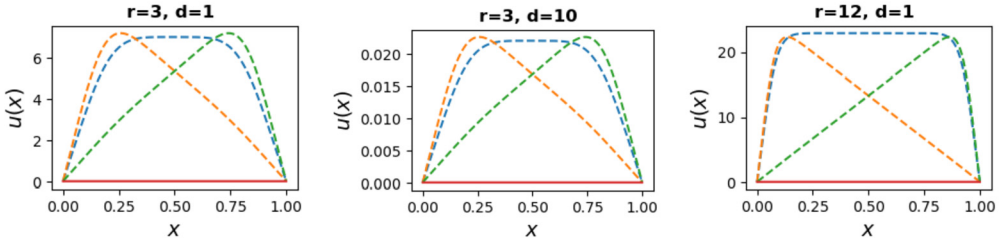

Fig. 6. Numerical solutions of Eq. (58) with $N = 1025$ grid points for different r and d. We have symmetric solutions so we only concern with one of them. Unstable solutions are plotted with dashed lines, while stable solutions are represented with solid lines.

Table 4
Computing time of homotopy method and CBMFEM vs. Number of Grid Points, N on **Example 2**. Both methods can find two solutions for this example.

N \ CPU time in sec	Homotopy Method	CBMFEM
3	0.005 s	0.006 s
4	0.009 s	N/A
5	0.016 s	0.09 s
6	0.029 s	N/A
7	0.05 s	N/A
8	0.10 s	N/A
9	0.25 s	0.09 s
10	0.50 s	N/A
11	1.53 s	N/A
12	2.84 s	N/A
13	6.52 s	N/A
14	24.76 s	N/A
15	30.78 s	N/A
16	73.88 s	N/A
17	272.95 s	0.09 s

Table 5
Computing time (in seconds) and the number of solutions of Eq. (57) for different p by CBMEFM with Newton's solver.

h	p = 1		p = 7		p = 18	
	CPUs	# of sols	CPUs	# of sols	CPUs	# of sols
2^{-2}	0.17	2	0.15	5	0.29	19
2^{-3}	0.12	2	0.35	9	3.01	37
2^{-4}	0.11	2	0.20	4	28.17	10
2^{-5}	0.11	2	0.11	4	0.38	8
2^{-6}	0.11	2	0.14	4	0.18	8
2^{-7}	0.14	2	0.23	4	0.33	8
2^{-8}	0.26	2	0.35	4	0.66	8
2^{-9}	0.57	2	0.95	4	1.93	8
2^{-10}	3.08	2	5.55	4	11.54	8

tensive computation caused by a large number of solution combinations on the higher level. Starting $\ell = 3$, we used Newton refinement with an interpolation initial guess from the coarse grid. We found 10 solutions and computed them until $h = 2^{-7}$. Since some solutions are the same up to the rotation, we plot only four solutions in Fig. 11. It is worth noting that Eq. (61) remains unchanged even when x is replaced by $1 - x$, and similarly for y. Therefore, rotating solutions 3 and 4 from Fig. 10 would

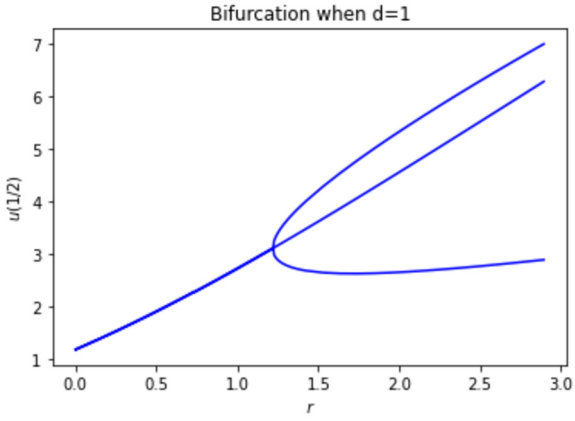

Fig. 7. Bifurcation diagram of Eq. (58) with respect to r with $N = 1025$ grid points and $d = 1$.

also yield valid solutions. Therefore, although there are 10 solutions in total, we only plot the 4 solutions in Fig. 10 up to the rotation. We also computed the numerical error and convergence order in both L^2 and H^1 norms for these solutions and summarized them in Table 11, the computing time is shown in Table 10.

Finally, we also explored the solution structure with respect to s in equation (61). We have used the homotopy continuation method to draw bifurcation diagrams. For small values of s, only two solutions are observed. However, as s increases, the number of solutions also increases, as demonstrated in Fig. 11.

5.2.2. The Gray–Scott model in 2D

The last example is the steady-state Gray-Scott model, given by

$$\begin{cases} -D_A \Delta A - SA^2 + (\mu + \rho)A = 0, & \text{in } \Omega \\ -D_S \Delta S + SA^2 - \rho(1 - S) = 0, & \text{in } \Omega \\ \dfrac{\partial A}{\partial \mathbf{n}} = \dfrac{\partial S}{\partial \mathbf{n}} = 0 & \text{in } \partial\Omega \end{cases} \tag{62}$$

$\Omega = (0, 1) \times (0, 1)$ and $\mathbf{n}$ is normal vector [19]. The solutions of this model depend on the constants D_A, D_S, μ, and ρ. In this example, we choose $D_A = 2.5 \times 10^{-4}$, $D_S = 5 \times 10^{-4}$, $\rho = 0.04$, and $\mu = 0.065$. Similar

Table 6
Numerical errors only nontrivial solutions for Eq. (57) when $p = 7$ by CBMEFM with Newton's solver.

h	# 1st solution				# 2nd solution				# 3rd solution			
	$\|e_H^h\|_{0,2}$	Order	$\|e_H^h\|_{1,2}$	Order	$\|e_H^h\|_{0,2}$	Order	$\|e_H^h\|_{1,2}$	Order	$\|e_H^h\|_{0,2}$	Order	$\|e_H^h\|_{1,2}$	Order
2^{-2}	1.6E-1	x	1.43	x	1.6E-1	x	9.0E-1	x	2.7E-2	x	1.1E-1	x
2^{-3}	2.4E-1	-0.54	1.22	0.23	3.3E-2	2.30	4.7E-1	0.93	6.8E-3	2.00	5.1E-2	1.08
2^{-4}	4.2E-2	2.52	7.4E-1	0.73	7.4E-3	2.13	2.2E-1	1.07	1.7E-3	2.00	2.5E-2	1.06
2^{-5}	8.4E-3	2.31	3.0E-1	1.28	1.9E-3	2.01	1.1E-1	1.01	4.3E-4	2.00	1.2E-2	1.03
2^{-6}	2.1E-3	2.04	1.4E-1	1.08	4.6E-4	2.00	5.5E-2	1.00	1.1E-4	2.00	5.9E-3	1.02
2^{-7}	5.1E-4	2.01	7.0E-2	1.03	1.2E-4	2.00	2.8E-2	1.00	2.7E-5	2.00	3.0E-3	1.01
2^{-8}	1.3E-4	2.00	3.5E-2	1.02	2.9E-5	2.00	1.4E-2	1.00	6.7E-6	2.00	1.5E-3	1.00
2^{-9}	3.2E-5	2.00	1.7E-2	1.01	7.2E-6	2.00	6.9E-3	1.00	1.7E-6	2.00	7.4E-4	1.00
2^{-10}	8.0E-6	2.00	8.6E-3	1.00	1.8E-6	2.00	3.5E-3	1.00	4.2E-7	2.00	3.7E-4	1.00

Table 7
Numerical errors only nontrivial solutions for Eq. (58) when $r = 3, d = 1$ by CBMEFM with Newton's solver.

h	# 1st solution				# 2nd solution			
	$\|e_H^h\|_{0,2}$	Order	$\|e_H^h\|_{1,2}$	Order	$\|e_H^h\|_{0,2}$	Order	$\|e_H^h\|_{1,2}$	Order
2^{-3}	1.3E-0	x	7.9E-0	x	1.0E-0	x	9.2E-0	x
2^{-4}	3.2E-1	2.04	4.2E-0	0.90	5.7E-1	0.87	5.4E-0	0.76
2^{-5}	8.0E-2	2.03	2.0E-0	1.06	1.1E-1	2.33	2.3E-0	1.22
2^{-6}	2.0E-2	2.03	1.0E-0	1.01	2.7E-2	2.03	1.2E-0	1.02
2^{-7}	4.9E-3	2.01	5.0E-1	1.00	6.7E-3	2.00	5.7E-1	1.00
2^{-8}	1.2E-3	2.00	2.5E-1	1.00	1.7E-3	2.00	2.9E-1	1.00
2^{-9}	3.1E-4	2.00	1.3E-1	1.00	4.2E-4	2.00	1.4E-1	1.00
2^{-10}	7.6E-5	2.00	6.3E-2	1.00	1.0E-4	2.00	7.2E-2	1.00

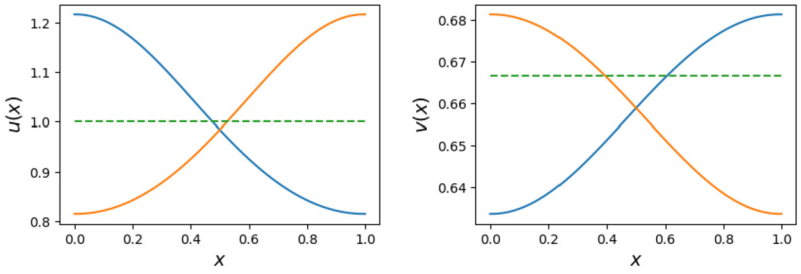

Fig. 8. 3 different solutions for equation (59) with $N = 1025$ grid points. The same colors are paired solutions.

Table 8
Numerical errors and computing time of CBMEFM with Newton's solvers for solving Eq. (59). We have symmetric solutions so we only concern with one of them.

h	# 1st solution				CPUs
	$\|e_H^h\|_{0,2}$	Order	$\|e_H^h\|_{1,2}$	Order	
2^{-3}	2.9E-2	x	1.9E-1	x	0.58
2^{-4}	6.3E-3	2.20	6.0E-2	1.63	0.42
2^{-5}	1.6E-3	2.02	2.7E-2	1.18	0.55
2^{-6}	3.9E-4	2.00	1.3E-2	1.06	0.84
2^{-7}	9.6E-5	2.00	6.3E-3	1.02	1.96
2^{-8}	2.4E-5	2.00	3.1E-3	1.01	6.14
2^{-9}	6.0E-6	2.00	1.6E-3	1.00	22.14
2^{-10}	1.5E-6	2.00	7.8E-4	1.00	157.88

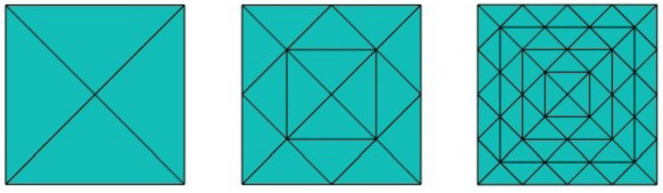

Fig. 9. Multi-level grid based on the edge refinement with a rectangular domain.

to the example of the Schnakenberg model in 1D (60), we can modify the system as follows:

Table 9
The number of nodes and triangles of the multigrid with the edge refinement for each level.

Step size	2^0	2^{-1}	2^{-2}	2^{-3}	2^{-4}	2^{-5}	2^{-6}	2^{-7}
# of Nodes	5	13	41	145	545	2113	8321	33025
# of Triangles	4	16	64	256	1024	4096	16384	65536

Table 10
The numerical performance summary of solving (61) with $s = 1600$. Until the level $\ell = 2$ we used CBMEFM and applied Newton's refinement starting from $\ell = 3$.

Method	Step size	# of solutions	Comp. Time
CBMEFM	2^0	2	0.2 s
	2^{-1}	10	1.4 s
	2^{-2}	10	142.7 s
Newton's refinement	2^{-3}	10	7.1 s
	2^{-4}	10	20.6 s
	2^{-5}	10	76.8 s
	2^{-6}	10	540.4 s
	2^{-7}	10	5521.3 s

$$\begin{cases} -D_A \Delta A - D_S \Delta S + (\mu + \rho)A - \rho(1 - S) = 0, \\ -D_S \Delta S + SA^2 - \rho(1 - S) = 0. \end{cases} \tag{63}$$

As the first equation in the Gray-Scott model is linear, we can solve for A in terms of S and substitute into the second equation to obtain a single polynomial equation. When using the companion matrix on the coarsest grid ($\ell = 0$) to solve the polynomial equation, we obtain 3^5

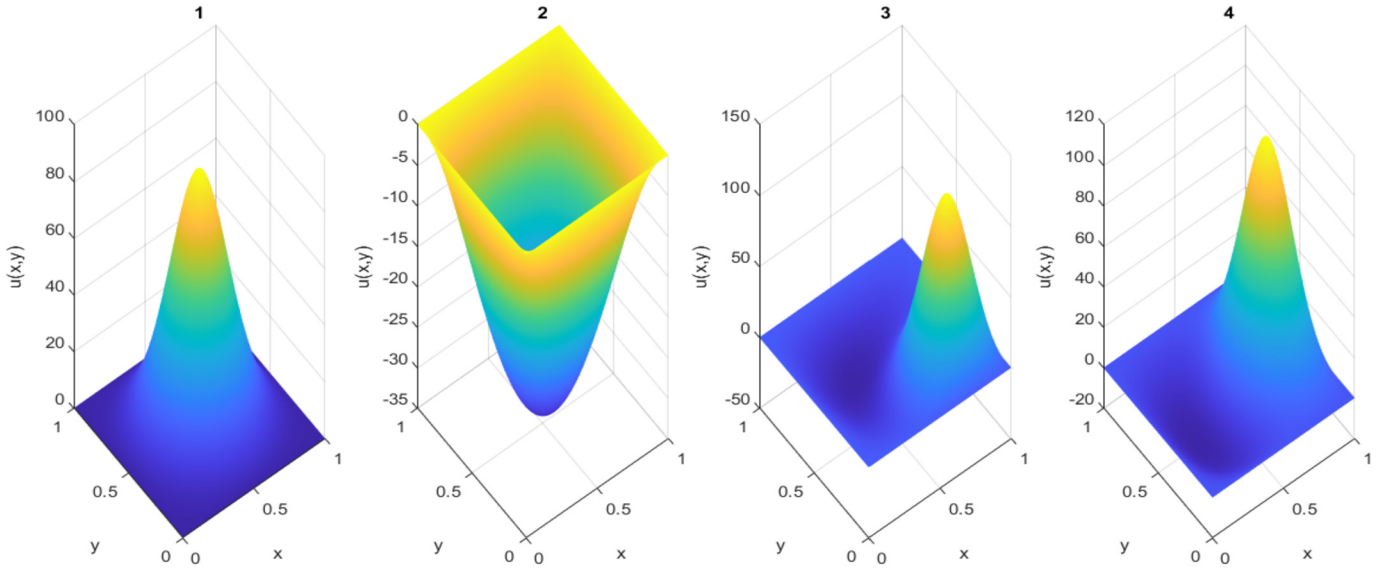

Fig. 10. Multiple solutions of Eq. (61) with $s = 1600$ and a step size of 2^{-7}.

Table 11
Numerical L^2 and H^1 errors for multiple solutions of Eq. (61) with $s = 1600$ shown in Fig. 10.

h	# 1st solution		# 2nd solution		# 3rd solution		# 4th solution	
	$\|e_u^h\|_{0,2}$	Order	$\|e_u^h\|_{0,2}$	Order	$\|e_u^h\|_{0,2}$	Order	$\|e_u^h\|_{0,2}$	Order
2^{-1}	2.1E-0	x	1.2E-0	x	x	x	x	x
2^{-2}	5.1E-0	-1.26	2.8E-0	-1.26	2.3E+1	x	5.4E-0	x
2^{-3}	3.9E-0	0.37	0.7E-0	1.94	9.5E-0	1.28	6.9E-0	-0.36
2^{-4}	1.6E-0	1.30	0.2E-0	1.98	3.2E-0	1.56	2.3E-0	1.58
2^{-5}	0.5E-0	1.70	0.5E-1	1.99	0.9E-0	1.85	0.7E-0	1.83
2^{-6}	0.1E-0	1.90	0.1E-1	2.00	0.2E-0	1.95	0.2E-0	1.95
2^{-7}	3.3 E-3	1.97	2.9E-03	2.00	0.6E-1	1.99	0.4E-1	1.99
h	$\|e_H^h\|_{1,2}$	Order	$\|e_H^h\|_{1,2}$	Order	$\|e_H^h\|_{1,2}$	Order	$\|e_H^h\|_{1,2}$	Order
2^{-1}	2.6E+1	x	1.4E+1	x	x	x	x	x
2^{-2}	6.8E+1	-1.40	2.7E+1	-0.93	1.9E+2	x	7.2E+1	x
2^{-3}	5.6E+1	0.29	1.5E+1	0.91	9.9E+1	0.92	7.9E+1	-0.13
2^{-4}	3.1E+1	0.86	7.4E-0	0.97	5.2E+1	0.92	4.2E+1	0.92
2^{-5}	1.6E+1	0.97	3.7E-0	0.99	2.6E+1	1.02	2.1E+1	1.01
2^{-6}	7.8E-0	1.00	1.9E-0	1.00	1.3E+1	1.01	1.0E+1	1.01
2^{-7}	3.9E-0	1.00	0.9E-0	1.00	6.3E-0	1.00	5.1E-0	1.00

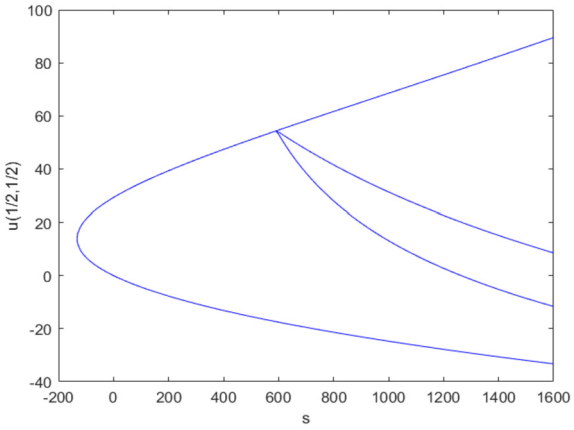

Fig. 11. Bifurcation diagram of solutions of Eq. (61) with respect to s.

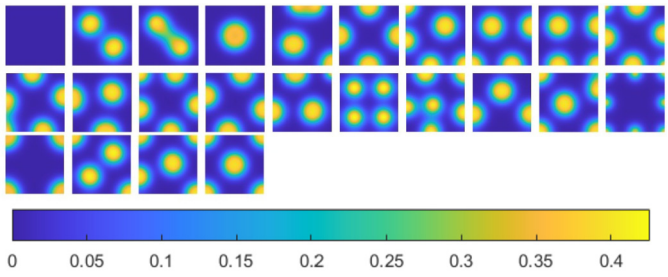

Fig. 12. We have 24 solutions and plot only $A(x, y)$ from (63) with a step size of 2^{-6}. The initial guesses were refined by considering both real solutions and real parts of complex solutions on the coarsest grid ($\ell = 0$).

complex solutions, leading to a large number of possible combinations on finer grids. To address this, we applied two approaches. The first approach involved keeping the real solutions and real parts of complex solutions, and using linear interpolation and Newton's method to refine them on finer grids. This approach yielded 24 solutions on a step size of 2^{-6}, up to rotation shown in Fig. 12. The second approach involved keeping only the real solutions, resulting in 1 solution on $\ell = 0$ and 3^{13} initial guesses on $\ell = 1$. Using interpolation and Newton's method, we obtained 88 solutions on a step size of 2^{-6}, up to rotation shown in Fig. 13. If we use more large coefficient for filtering conditions we can get 187 solutions.

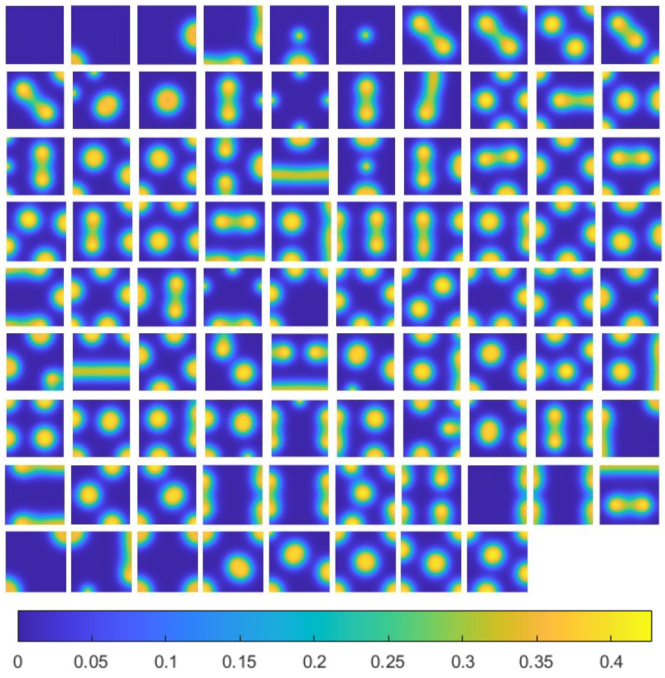

Fig. 13. We have 88 solutions and plot only $A(x, y)$ from (63) with a step size of 2^{-6}. The initial guesses were refined by considering only the real solutions on the $\ell = 1$ grid.

6. Conclusion

In this paper, we have presented a novel approach, the Companion-Based Multilevel finite element method (CBMFEM), which efficiently and accurately generates multiple initial guesses for solving nonlinear elliptic semi-linear equations with polynomial nonlinear terms together with its theoretical foundation. In particular, our numerical results demonstrate the consistency of the method with theoretical analysis, and we have shown that CBMFEM outperforms existing methods for problems with multiple solutions.

CBMFEM has potential applications in more complex PDEs, posed both in 2D and 3D, which arise from a variety of scientific and engineering fields. To tackle such cases, we shall need to conduct in-depth investigations to identify better filtering condition constants and better nonlinear solvers. As an immediate enhancement or extension of our method, we shall incorporate the multigrid method to speed up the Newton method and attempt to handle PDEs posed on a complicated geometry in our future works.

Declarations

WH and SL are supported by NIH via 1R35GM146894 and NSF DMS-2052685. YL is supported by NSF via DMS 2208499.

Data availability

No data was used for the research described in the article.

References

[1] Ivo Babuska, Survey lectures on the mathematical foundations of the finite element method, in: The Mathematical Foundations of the Finite Element Method with Applications to Partial Differential Equations, 1972, pp. 3–359.
[2] Daniel J. Bates, Andrew J. Sommese, Jonathan D. Hauenstein, Charles W. Wampler, Numerically Solving Polynomial Systems with Bertini, SIAM, 2013.
[3] Achi Brandt, Oren E. Livne, Multigrid Techniques: 1984 Guide with Applications to Fluid Dynamics, revised edition, SIAM, 2011.
[4] Susanne C. Brenner, Ridgway Scott, The Mathematical Theory of Finite Element Methods, vol. 15, Springer Science & Business Media, 2008.
[5] B. Breuer, P. Joseph McKenna, Michael Plum, Multiple solutions for a semilinear boundary value problem: a computational multiplicity proof, J. Differ. Equ. 195 (1) (2003) 243–269.
[6] Mingchao Cai, Mo Mu, Jinchao Xu, Numerical solution to a mixed Navier–Stokes/Darcy model by the two-grid approach, SIAM J. Numer. Anal. 47 (5) (2009) 3325–3338.
[7] ChuanMiao Chen, ZiQing Xie, Analysis of search-extension method for finding multiple solutions of nonlinear problem, Sci. China Ser. A, Math. 51 (1) (2008) 42–54.
[8] Long Chen, Xiaozhe Hu, Steven Wise, Convergence analysis of the fast subspace descent method for convex optimization problems, Math. Comput. (2020).
[9] Y.S. Choi, P.J. McKenna, M. Romano, A mountain pass method for the numerical solution of semilinear wave equations, Numer. Math. 64 (1) (1993) 487–509.
[10] Monique Dauge, Neumann and mixed problems on curvilinear polyhedra, Integral Equ. Oper. Theory 15 (1992) 227–261.
[11] Andreas Deutsch, Sabine Dormann, Mathematical Modeling of Biological Pattern Formation, Springer, 2005.
[12] Lawrence C. Evans, Weak Convergence Methods for Nonlinear Partial Differential Equations, vol. 74, American Mathematical Soc., 1990.
[13] Patrick E. Farrell, A. Birkisson, Simon W. Funke, Deflation techniques for finding distinct solutions of nonlinear partial differential equations, SIAM J. Sci. Comput. 37 (4) (2015) A2026–A2045.
[14] Alessio Figalli, The Monge-Ampère equation and its applications, 2020.
[15] Philippe Grandclément, Jérôme Novak, Spectral methods for numerical relativity, Living Rev. Relativ. 12 (2009) 1–103.
[16] Cristian E. Gutiérrez, Haim Brezis, The Monge-Ampere Equation, vol. 44, Springer, 2001.
[17] Wenrui Hao, Jonathan D. Hauenstein, Bei Hu, Andrew J. Sommese, A bootstrapping approach for computing multiple solutions of differential equations, J. Comput. Appl. Math. 258 (2014) 181–190.
[18] Wenrui Hao, Jan Hesthaven, Guang Lin, Bin Zheng, A homotopy method with adaptive basis selection for computing multiple solutions of differential equations, J. Sci. Comput. 82 (2020) 1–17.
[19] Wenrui Hao, Chuan Xue, Spatial pattern formation in reaction–diffusion models: a computational approach, J. Math. Biol. 80 (2020) 521–543.
[20] Wenrui Hao, Chunyue Zheng, An adaptive homotopy method for computing bifurcations of nonlinear parametric systems, J. Sci. Comput. 82 (3) (2020) 1–19.
[21] Van Henson, et al., Multigrid methods nonlinear problems: an overview, Comput. Imaging 5016 (2003) 36–48.
[22] Peiqi Huang, Mingchao Cai, Feng Wang, A Newton type linearization based two grid method for coupling fluid flow with porous media flow, Appl. Numer. Math. 106 (2016) 182–198.
[23] Douglas Samuel Jones, Michael Plank, Brian D. Sleeman, Differential Equations and Mathematical Biology, CRC Press, 2009.
[24] Todd Kapitula, Panayotis G. Kevrekidis, Björn Sandstede, Counting eigenvalues via the Krein signature in infinite-dimensional Hamiltonian systems, Phys. D: Nonlinear Phenom. 195 (3–4) (2004) 263–282.
[25] Panayotis G. Kevrekidis, Dimitri J. Frantzeskakis, Ricardo Carretero-González, The Defocusing Nonlinear Schrödinger Equation: from Dark Solitons to Vortices and Vortex Rings, SIAM, 2015.
[26] J. Lega, J.V. Moloney, A.C. Newell, Swift-Hohenberg equation for lasers, Phys. Rev. Lett. 73 (22) (1994) 2978.
[27] Dmitriy Leykekhman, Buyang Li, Maximum-norm stability of the finite element Ritz projection under mixed boundary conditions, Calcolo 54 (2) (2017) 541–565.
[28] Zhaoxiang Li, Zhi-Qiang Wang, Jianxin Zhou, A new augmented singular transform and its partial Newton-correction method for finding more solutions, J. Sci. Comput. 71 (2017) 634–659.
[29] John M. Neuberger, James W. Swift, Newton's method and Morse index for semilinear elliptic pdes, Int. J. Bifurc. Chaos 11 (03) (2001) 801–820.
[30] Paul H. Rabinowitz, et al., Minimax Methods in Critical Point Theory with Applications to Differential Equations, American Mathematical Soc., 1986.
[31] Alfred Schatz, Junping Wang, Some new error estimates for Ritz–Galerkin methods with minimal regularity assumptions, Math. Comput. 65 (213) (1996) 19–27.
[32] L. Ridgway Scott, Shangyou Zhang, Finite element interpolation of nonsmooth functions satisfying boundary conditions, Math. Comput. 54 (190) (1990) 483–493.
[33] Horatiu Simon, Concentration for one and two-species one-dimensional reaction-diffusion systems, J. Phys. A, Math. Gen. 28 (23) (1995) 6585.
[34] Vitaly Volpert, Elliptic Partial Differential Equations: Volume 2: Reaction-Diffusion Equations, vol. 104, Springer, 2014.
[35] Yingwei Wang, Wenrui Hao, Guang Lin, Two-level spectral methods for nonlinear elliptic equations with multiple solutions, SIAM J. Sci. Comput. 40 (4) (2018) B1180–B1205.
[36] Zhi-Qiang Wang, Jianxin Zhou, A local minimax-Newton method for finding multiple saddle points with symmetries, SIAM J. Numer. Anal. 42 (4) (2004) 1745–1759.
[37] Juncheng Wei, Matthias Winter, Mathematical Aspects of Pattern Formation in Biological Systems, vol. 189, Springer Science & Business Media, 2013.
[38] Ziqing Xie, Yongjun Yuan, Jianxin Zhou, On solving semilinear singularly perturbed Neumann problems for multiple solutions, SIAM J. Sci. Comput. 44 (1) (2022) A501–A523.
[39] Jinchao Xu, A novel two-grid method for semilinear elliptic equations, SIAM J. Sci. Comput. 15 (1) (1994) 231–237.

[40] Jinchao Xu, Two-grid discretization techniques for linear and nonlinear pdes, SIAM J. Numer. Anal. 33 (5) (1996) 1759–1777.
[41] Xuefeng Xu, Chen-Song Zhang, Convergence analysis of inexact two-grid methods: a theoretical framework, SIAM J. Numer. Anal. 60 (1) (2022) 133–156.
[42] Xuefeng Xu, Chen-Song Zhang, A new analytical framework for the convergence of inexact two-grid methods, SIAM J. Matrix Anal. Appl. 43 (1) (2022) 512–533.
[43] Jianyuan Yin, Bing Yu, Lei Zhang, Searching the solution landscape by generalized high-index saddle dynamics, Sci. China Math. 64 (2021) 1801–1816.
[44] Jianyuan Yin, Lei Zhang, Pingwen Zhang, High-index optimization-based shrinking dimer method for finding high-index saddle points, SIAM J. Sci. Comput. 41 (6) (2019) A3576–A3595.
[45] Xinyue Evelyn Zhao, Long-Qing Chen, Wenrui Hao, Yanxiang Zhao, Bifurcation analysis reveals solution structures of phase field models, Commun. Appl. Math. Comput. Sci. (2022) 1–26.